JOURNAL OF SOLID STATE CHEMISTRY **131,** 317–325 (1997)
ARTICLE NO. SC977387

Bonding and Structural Variations in Doped $Bi_2Sn_2O_7$

Ismunandar and Brendan J. Kennedy

School of Chemistry, The University of Sydney, Sydney, New South Wales 2006, Australia

Brett A. Hunter

Australian Nuclear Science and Technology Organisation, P.M.B. 1, Menai, New South Wales 2234, Australia

and

Tom Vogt

Department of Physics, 510B, Brookhaven National Laboratory, Upton, New York

Received October 9, 1996; in revised form March 10, 1997; accepted March 11, 1997

The structural properties of Y-doped $Bi_2Sn_2O_7$ have been determined by Rietveld analysis of powder neutron and synchrotron X-ray diffraction data. These materials form a series of cubic pyrochlore-type oxides with a distinct miscibility gap at low Bi contents and show large deviations from Vegards law. Temperature-dependent structural studies of (BiY)Sn_2O_7 and (BiYb)Sn_2O_7 have been undertaken. The structure of the high temperature, pyrochlore phase of $Bi_2Sn_2O_7$ has been refined using powder neutron diffraction data. The evolution of the charge density on the Bi site has been probed using a combination of bond valence sum calculations and electronic spectroscopy.

INTRODUCTION

Bismuth-containing oxides are of considerable importance as heterogeneous catalysts for a variety of processes including the oxidative coupling of methane, the ammoxidation of propylene, and the oxidation of hydrocarbons, carbohydrates and CO (1–4). They are also used as sensors (5) and as electrode materials in the reduction of oxygen (6, 7). This wide range of chemical reactivity can be partially understood as being related to the $6s^2$ lone pair electrons of Bi(III). The Bi 6*s* electrons are believed to be crucial in controlling surface valence fluctuations and in stabilizing the oxygen non stiochiometry necessary for Bi-containing oxides to act as oxygen transfer catalysts. In ternary oxides the Bi $6s^2$ electrons can modify the bonding of other *M*–O networks. This behavior is well illustrated in the pyrochlore-type ruthenate oxides. In $Bi_2Ru_2O_7$ the Ru 4*d* electrons are delocalized and the material is a metallic conductor, whereas $Y_2Ru_2O_7$ is a semiconducting oxide (8, 9).

By a systematic investigation of the structural properties of complex oxides it should be possible to identify features associated with high catalytic activity and selectivity. Unfortunately, relatively few materials form suitably large arrays of structurally related metal oxides necessary to probe the often subtle factors characterizing an optimal catalyst. An exception is the ternary tin oxides which form an extensive array of pyrochlore-type oxides (10). Pyrochlore oxides, of the general type $A_2B_2O_6O'$, have a number of features attractive for designing catalysts, including the ease of substitution, the formation of oxygen vacancies, and high temperature stability. The pyrochlore structure is usually described as two interpenetrating three-dimensional networks, a B_2O_6 network composed of corner-sharing BO_6 octahedra and a A_2O' network of corner-linked A_4O tetrahedra. These two networks interact only weakly and vacancies on the special oxygen site (O′) are common (10).

The activity of bismuth–tin oxides both as a sensor and as a catalyst for the partial oxidation of methane has recently been studied by a number of groups (5, 11–14). Unlike the lanthanide–tin oxides, which invariably adopt the archetypal cubic pyrochlore structure, $Bi_2Sn_2O_7$ only adopts the regular pyrochlore structure at high temperatures (15). At lower temperatures the precise structure of $Bi_2Sn_2O_7$ is not well established—conflicting reports suggest that the structure is sensitive to the precise stoichiometry and is easily modified by various impurities (15–17). Pure $Bi_2Sn_2O_7$ appears to be tetragonal at room temperature with $a = 15.10$, $c = 21.5$ Å. It is unclear what, if any, role the Bi 6*s* electrons play in stabilizing the tetragonal pyrochlore-type structure.

The current work presents a detailed analysis of the structure and bonding of Y- and Yb-doped $Bi_2Sn_2O_7$ as part of a wider study of the structure and bonding in

0022-4596/97 $25.00

pyrochlore oxides (6, 18–22). The high-temperature structure of the pyrochlore phase of $Bi_2Sn_2O_7$ has also been determined using powder neutron diffraction data. The aims of the present work were twofold, first to establish if the Bi 6s electrons are sterochemically active in these materials and second to determine how structural changes in the pyrochlores influence the electronic properties of Bi(III).

EXPERIMENTAL

The samples $(Bi_{2-\delta}Y_\delta)Sn_2O_7$ and $(BiYb)Sn_2O_7$ were prepared by solid state reaction from mixtures of Bi_2O_3, Y_2O_3, Yb_2O_3, and SnO_2 in the appropriate molar ratios. Each mixture was heated in air at up to 1400°C for 4 days with intermittent grinding. The process was monitored using X-ray diffraction (XRD) to ensure complete reaction at which time the mixtures were fired at 1400°C for an additional 2 days. In the case of $Bi_2Sn_2O_7$ the maximum temperature used was 1000°C.

Preliminary powder XRD patterns were recorded using Ni-filtered Cu$K\alpha$ radiation on a Siemens D5000 diffractometer. High-resolution patterns were recorded at $\lambda =$ 1.00 Å using image plate detectors on the Debye–Scherrer camera at the Australian National Beamline Facility (beamline 20B) at the Photon Factory, Tsukuba, Japan. Samples were finely ground and packed in glass capillaries and rotated at the center of the instrument using a custom built sample spinner. A full description of the instrument has been given elsewhere (23, 24).

Powder neutron diffraction data for $(BiY)Sn_2O_7$ and $(BiYb)Sn_2O_7$ were collected at various temperatures on the high-resolution neutron powder diffractometer (HRNPD) at the High Flux Beam Reactor, Brookhaven National Laboratory (25), using neutrons of wavelength 1.8857 Å. Data for $Bi_2Sn_2O_7$ was collected at 850°C using neutrons of wavelength 1.4925 Å on the powder diffractometer at the Australian Nuclear Science and Technology Organization's HIFAR reactor (26). The Rietveld refinements were carried out using the computer program PROFIL (27) or LHPM (28). For the neutron diffraction analysis no absorption correction was performed, while for the X-ray data analysis the absorption correction described by Sabine was used (29). The neutron scattering lengths used were Bi, 8.5256; Y, 7.750; Yb, 12.900; Sn, 6.2170; and O, 5.805 fm. Further details are given in Tables 1–5.

Solid state electronic spectra were recorded at room temperature on a Cary 5E UV–visible/NIR spectrometer. Bond valence sum and Madelung site potentials were calculated using the program EUTAX (30).

RESULTS AND DISCUSSION

The room temperature powder XRD pattern of a sample of $Bi_2Sn_2O_7$ prepared using standard methods could be indexed on the basis of a tetragonal cell with $a = \sqrt{2}a' =$ 15.1007 and $c = 2a' = 21.5536$ Å, where a' is the size of the cubic pyrochlore. A temperature-dependent XRD study showed that above 850°C $Bi_2Sn_2O_7$ adopts a regular pyrochlore structure, space group $Fd\bar{3}m$, in which the larger Bi(III) cations occupy the 16*d* positions at (0.5, 0.5, 0.5) and the smaller Sn(IV) cations the 16*c* positions at (0, 0, 0). There are two types of oxygen, one at the 48*f* sites (x, 0.125, 0.125) and the other at the 8*b* sites (0.375, 0.375, 0.375). In the present case both oxygen sites are fully occupied. The structure of the high-temperature pyrochlore phase was refined from powder neutron diffraction data collected at 850°C with $a = 10.7428(4)$ Å and $x = 0.3255(4)$. Further details are given in Table 1. The Sn–O distance of 2.065(3) Å is marginally longer than that found in other pyrochlore oxides where it is around 2.04–2.05 Å (20, 21). This distance

TABLE 1
Atomic Coordinates and Thermal Parameters for $Bi_2Sn_2O_7$ at 850°C

Atom	Site	x	y	z	B_{iso} (Å^3)
Bi	16*d*	0.5	0.5	0.5	6.7(1)
Sn	16*c*	0	0	0	1.3(1)
O	48*f*	0.3255(4)	0.125	0.125	3.0(1)
O′	8*b*	0.375	0.375	0.375	4.8(3)

Note. Space group $Fd\bar{3}m$ (No. 277), $a = 10.7428(4)$ Å, $V = 1239.8$ Å^3. R_p, 4.86; R_{wp}, 6.20; R_{exp}, 3.80. Estimated standard deviations are in parentheses.

TABLE 2
Atomic Coordinates and Thermal Parameters for $(Bi_{2-\delta}Y_\delta)Sn_2O_7$ at Room Temperature

δ	Phase	a (Å)	x #[b]	R_p	R_{wp}	GOF
0.6		10.4816(4)	0.3324(3)	2.62	3.38	15.14
0.8		10.4142(3)	0.3272(5)	2.27	2.93	14.08
		10.4000(3)	0.3411(1)			
1.0		10.5025(3)	0.349(1)	3.23	4.13	23.42
1.2[a]	β	10.4189(5)	0.3392(8)	3.16	4.38	32.77
	α	10.3746(5)	0.338(1)			
1.4[a]	β	10.4147(5)	0.3346(4)	3.99	5.19	25.13
	α	10.3786(5)	0.3367(8)			
1.6[a]	α	10.3697(2)	0.3337(3)	3.37	4.29	23.93
	$Y_2Sn_2O_7$	10.3402(2)	0.3370(5)			
1.8	α	10.3563(3)	0.3394(6)	3.76	5.07	34.99
	$Y_2Sn_2O_7$	10.3360(2)	0.3342(2)			

Note. Space group $Fd\bar{3}m$. Estimated standard deviations are in parentheses.

[a] Trace amount of SnO_2 also present in the sample.

[b] x parameter for O(1). All other positional parameters as in Table 1.

TABLE 3
Atomic Coordinates and Thermal Parameters for $(Bi_{2-\delta}Y_\delta)Sn_2O_7$ at Room Temperature

δ	a (Å)	Bi/Y	Sn	O(1)	O(2)	O(3)	O(4)	R_p	R_{wp}	GOF
		(x, x, x)	(x, x, x)	$(x, 0, 0)$	$(x, 1/4, 1/4)$	$(3/4, 3/4, 3/4)$	$(0, 0, 0)$			
0.4	10.5332(2)	0.8766(1)	0.3717(1)	0.296(1)	0.472(1)	0.75	0	3.47	4.49	21.00
0.2	10.6143(2)	0.8764(1)	0.3670(1)	0.305(1)	0.461(1)	0.75	0	5.53	7.31	9.42

Note. Space group $F\bar{4}\,3m$. Estimated standard deviations are in parentheses.

is not unreasonably long since, for example, the average Sn–O distance in Li_2SnO_3 is 2.072 Å (31). The two Bi–O distances, 2.669 and 2.326 Å, are both noticeably longer than those found in the metallic oxides $Bi_2Ir_2O_7$ and $Bi_2Ru_2O_7$ (19, 22). The single variable oxygen positional parameter, x, is noticeably smaller than that found in other stannate pyrochlores such as $Y_2Sn_2O_7$ and $Yb_2Sn_2O_7$, where it is 0.3369(1) and 0.3391(1), respectively (20, 21).

Powder XRD measurements of the series $(Bi_{2-\delta}Y_\delta)Sn_2O_7$, where $\delta = 0, 0.2, 0.4, \ldots, 2$, revealed a discontinuity in the lattice parameter versus composition plot near $\delta = 1$ (Fig. 1). Using a conventional laboratory-based Bragg–Brentano diffractometer the materials seem to form two series of solid solutions with $\delta > 1$ and $\delta < 1$. High-resolution measurements with $\lambda = 1.00$ Å using a synchrotron-based Debye–Scherrer camera over the range $10 < d < 0.56$ Å confirmed the formation of a series of highly crystalline materials best described as a solid solution $(Bi_{2-\delta}Y_\delta)Sn_2O_7$ for the Bi-rich compounds with $\delta < 1$. For these compounds the lattice parameter uniformly decreases with increasing δ in accordance with Vegard's law. However the diffraction patterns of the Y-rich compounds $\delta > 1$ reveal (Fig. 2) a splitting of all the Bragg reflections and the Rietveld analysis demonstrated that the samples consist of two pyrochlore-type oxides with very similar lattice parameters (Table 2). It is clear from Fig. 1 that $(BiY)Sn_2O_7$ does not fall into either category.

The results of the Rietveld refinement from the synchrotron XRD data are summarized in Tables 2 and 3. For some of the Y-rich compounds additional weak reflections due to the presence of SnO_2 were also observed. This phase was included in the analysis. Two distinct Bi-doped $Y_2Sn_2O_7$ compounds appear to form, α-$Y_2Sn_2O_7$ with $a = 10.400(5)$ Å and β-$Y_2Sn_2O_7$ with $a = 10.445(5)$ Å. At low Bi contents the sample consists of a mixture of undoped $Y_2Sn_2O_7$ ($a = 10.370$ Å) and lightly Bi-doped α-$Y_2Sn_2O_7$ while at higher Bi contents a mixture of the α and, the more heavily doped, β phases are formed. It was not possible to index the diffraction data with a unit cell of lower symmetry. Attempts to determine the precise Bi contents of the two phases were inconclusive. Analysis clearly demonstrates that a three-phase mixture of $Y_2Sn_2O_7$ plus the α and β phases is not present. At high Bi contents a series of single-phase pyrochlore-type materials, that are best described as Y-doped $Bi_2Sn_2O_7$, were formed. It appears that while the larger $Bi_2Sn_2O_7$ lattice has enough flexibility to accommodate infinitely variable amounts of the smaller Y atoms, indeed that the addition of Y stabilizes a cubic pyrochlore-type polymorph with respect to the tetragonal form, Bi cannot substitute randomly for Y in the host $Y_2Sn_2O_7$ lattice but rather forms discrete pyrochlore phases. The present results are in contrast to the previous study by Knop who reported that pyrochlore-type materials were not formed in Bi–Y–Sn oxides (32).

Careful examination of the diffraction patterns of $(Bi_{1.8}Y_{0.2})Sn_2O_7$ and $(Bi_{1.6}Y_{0.4})Sn_2O_7$ revealed a number of additional lines that could be indexed on the basis of a 10.6 Å cubic cell, but are inconsistent with the regular pyrochlore structure. Two possibilities, where the Bi $6s^2$ electrons become sterochemically active, were considered. The simplest possibility is that the space group remains $Fd\bar{3}m$ but the Bi is displaced from the 16*d* position onto half of a nearby 32*e* position at (x, x, x) while the tin and oxygen atoms remain in the standard pyrochlore-type positions. This model failed to account for all the extra reflections. In the second model the Bi is again displaced along the [111] direction, so that there are alternate long–short Bi–O bonds in the Bi_2O' chains, but now the tin and oxygen atoms are also displaced. This was modeled in space group $F\,\bar{4}3m$ and, as is clear from Fig. 3, this model accounts for all the extra reflections. For both compounds the Bi is displaced about 0.03 Å toward O(4); the Bi–O(3) distance is about 0.05 Å longer than the Bi–O(4) distance (Table 3). We propose that the Bi 6*s* electrons are preferentially located between Bi and O(3) in these two oxides.

TABLE 4
Selected Bond Distances for $(Bi_{2-\delta}Y_\delta)Sn_2O_7$, $\delta = 0.2$ and 0.4

Bond	$\delta = 0.2$ (Å)	$\delta = 0.4$ (Å)
Bi/Y–O(1)	2.67(1)	2.59(1)
Bi/Y–O(2)	2.57(1)	2.47(1)
Bi/Y–O(3)	2.325(1)	2.310(1)
Bi/Y–O(4)	2.272(1)	2.251(1)
Sn–O(1)	2.071(4)	2.071(3)
Sn–O(2)	2.043(7)	2.096(7)

Note. Estimated standard deviations are in parenthesis.

TABLE 5
Atomic Coordinates and Thermal Parameters for $(Bi_{2-\delta}Y_{\delta})Sn_2O_7$

				B_{iso} (Å)^2					
T (K)	a (Å)	x	A^a	Sn	O	O′	R_{wp}	R_I	R_{exp}
				$(BiY)Sn_2O_7$					
10	10.4911(2)	0.3324(2)	1.72(7)	0.28(7)	1.1(2)	0.67(4)	10.7	6.2	5.1
50	10.4908(2)	0.3322(2)	1.60(7)	0.29(7)	1.0(2)	0.66(4)	10.8	5.8	5.2
100	10.4919(2)	0.3320(2)	1.60(7)	0.33(7)	0.9(2)	0.69(4)	11.1	6.2	5.2
200	10.4961(2)	0.3319(2)	1.72(8)	0.36(7)	0.8(2)	0.71(4)	10.9	5.7	5.4
295	10.5022(2)	0.3323(2)	1.84(8)	0.61(6)	1.2(1)	0.96(3)	10.0	5.3	5.7
				$(BiYb)Sn_2O_7$					
10	10.4536(5)	0.3327(2)	1.20(5)	0.28(7)	0.8(2)	0.54(3)	10.6	4.8	5.6
50	10.4543(5)	0.3332(2)	1.37(5)	0.42(8)	1.1(2)	0.65(3)	10.5	5.2	5.6
100	10.4557(5)	0.3330(2)	1.48(6)	0.32(8)	0.9(2)	0.66(3)	10.6	5.4	5.7
200	10.4595(5)	0.3332(2)	1.43(5)	0.31(7)	0.7(2)	0.68(3)	10.5	4.6	5.7
295	10.4661(4)	0.3336(2)	1.56(4)	0.24(6)	1.1(2)	0.73(3)	8.2	3.7	4.9

Note. Space group $Fd\,\bar{3}\,m$. Estimated standard deviations are in parentheses. Refinement results on neutron powder diffraction data for $(BiY)Sn_2O_7$ and $(BiYb)Sn_2O_7$. Other positional parameters are as given in Table 1.

[a] Thermal parameters for the atoms occupying the pyrochlore A site were constrained to be equal.

A second feature seen in Fig. 1 is the apparent "anomalous" lattice parameter observed for $(BiY)Sn_2O_7$. In this sample while some very weak reflections due to SnO_2 were observed, corresponding to less than 0.5 wt%, the synchrotron XRD data clearly demonstrate the major species present in the sample to be a cubic pyrochlore. Since pure $Bi_2Sn_2O_7$ undergoes at least one temperature-dependent phase transition, with the pyrochlore phase only being observed at high temperatures, a temperature-dependent structural study of $(BiY)Sn_2O_7$ was performed. In this case powder neutron diffraction patterns were collected to probe any temperature-dependent displacements of the oxygen atoms. $(BiY)Sn_2O_7$ retains a simple pyrochlore structure over the temperature range studied (10–300 K) (Fig. 4). The cubic lattice parameter increases regularly as the temperature is increased (Fig. 5), while x decreases slightly with increasing lattice size.

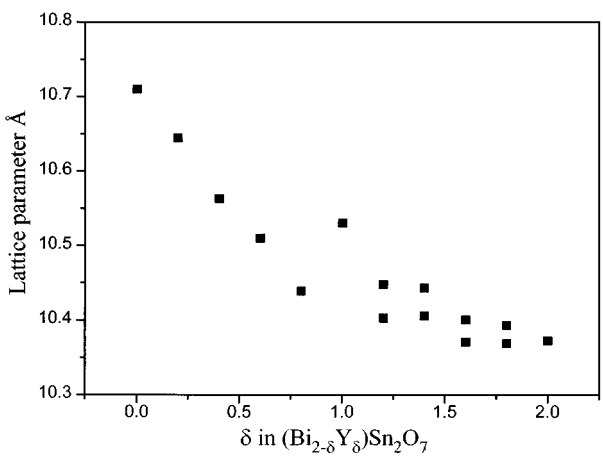

FIG. 1. Variation of the lattice parameter as a function of composition for the complexes $(Bi_{2-\delta}Y_{\delta})Sn_2O_7$ as determined from synchrotron X-ray diffraction data.

Given that the above data offers little, if any, structural evidence to rationalize either the stability of a distorted pyrochlore structure in $Bi_2Sn_2O_7$ at room temperature or the "anomalous" lattice parameter of $(BiY)Sn_2O_7$, it is likely that these changes are electronic in origin. The Bi(III) $6s^2$ lone pair of electrons can either be sterochemically active as for $Bi_{1.8}Y_{0.2}Sn_2O_7$ or BiI_3 (33) or they may be involved in M–O bonding as in $Bi_2Ru_2O_7$ (8, 19). In the pyrochlores the Bi coordination geometry is best described as a compressed $BiO_6O'_2$ scalehedron in which there are two short Bi–O′ bonds and six longer Bi–O bonds. The Bi site symmetry ($\bar{3}m$) in the pyrochlore structure is apparently inconsistent with a sterochemically active lone pair. It is possible that the Bi $6s^2$ electrons are directed along the threefold axis, randomly pointing either toward or away from one of the two short Bi–O′ bonds thus lengthening the average Bi–O′ bonds without changing the symmetry. The BiO_8 scalehedron in $Bi_2Sn_2O_7$ is considerably larger than that in the analogous Ru or Ir pyrochlores where the Bi $6s^2$ electrons are involved in the M–O–M bonding. The expansion of the BiO_8 scalehedron in $Bi_2Sn_2O_7$ does not involve a simple elongation along the threefold axis of the type described above, but rather both the Bi–O and Bi–O′ distances increase. In the semi-conducting pyrochlore $Bi_2Pt_2O_7$ (34) the Bi 6s electrons are not involved in the bonding and the corresponding Bi–O bond distances,

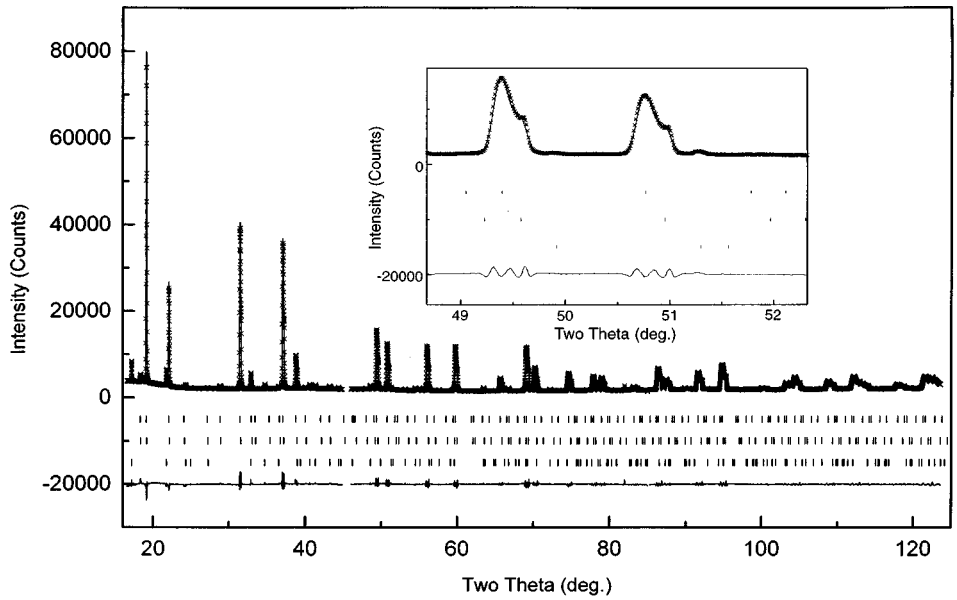

FIG. 2. Observed (x), calculated, and difference (full line) diffraction profiles of $(Bi_{0.6}Y_{1.4})Sn_2O_7$. The short vertical marks show the positions of the allowed Bragg reflections for the two pyrochlore-type phases and of the SnO_2 (bottom set) impurity phase. The insert illustrates the splitting of the reflection due to the presence of the two pyrochlore phases. The gaps near 45° and 85° result from the use of image plate detectors.

obtained from powder XRD data, are somewhat shorter, 2.40 and 2.25 Å, suggesting that there may in fact be a slight contraction along the threefold axis.

For the ideal compounds $Bi_2Sn_2O_7$, $(BiY)Sn_2O_7$, and $Y_2Sn_2O_7$, for which precise values of x are available from powder neutron diffraction studies, x increases almost linearly with a (Table 6). Within the limitation of the small number of samples both the A–O and A–O′ distances also increase linearly with the cubic lattice parameter. For the A–O′ distance the linear dependence on a is a consequence of the local geometry, this distance being given by $(a\sqrt{3}/8)$. The biggest deviation from a simple linear relationship is seen for the Sn–O distances. In both $Y_2Sn_2O_7$ and $(BiY)Sn_2O_7$ the Sn–O distance is about 2.04 Å, which is the

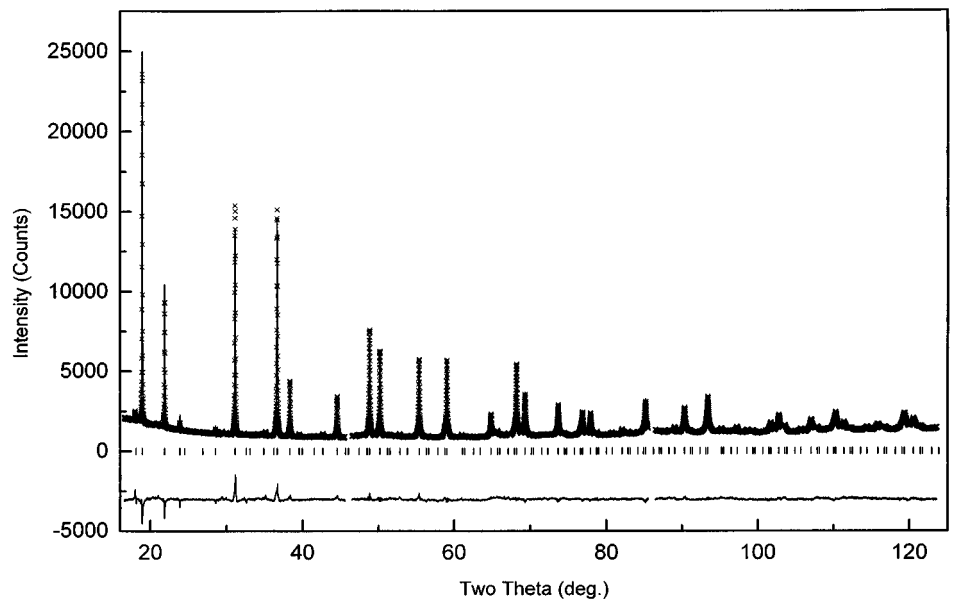

FIG. 3. Observed (x), calculated, and difference (full line) diffraction profiles of $(Bi_{1.6}Y_{0.4})Sn_2O_7$. The short vertical lines below the profiles mark the position of all possible Bragg reflections.

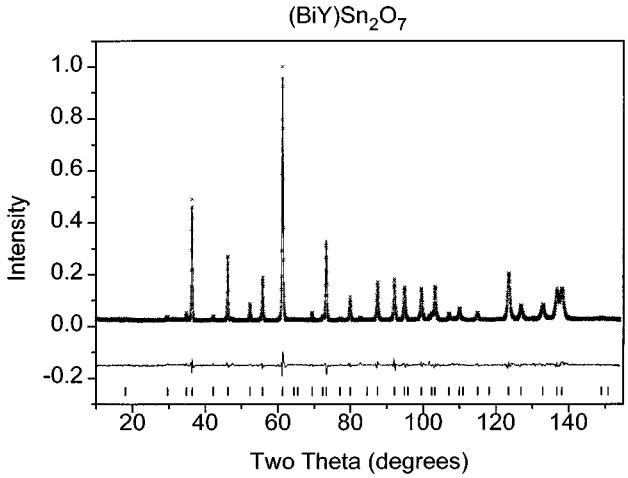

FIG. 4. Room temperature powder neutron diffraction pattern for $(BiY)Sn_2O_7$. The format is the same as in Fig. 3.

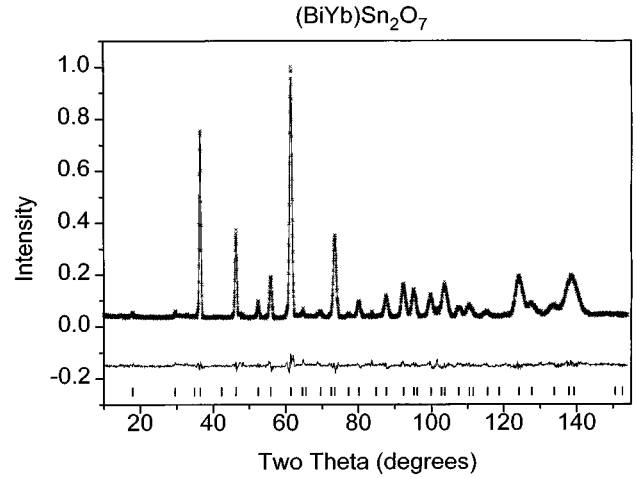

FIG. 6. Room temperature powder neutron diffraction pattern for $(BiYb)Sn_2O_7$. The format is the same as in Fig. 3.

minimum Sn–O distance possible in this structure type. In $Bi_2Sn_2O_7$ the corresponding distance is noticeably longer, however examination of a number of pyrochlore structures shows (10, 18, 20) that this is a consequence of the larger cell volume and is not due to any electronic effects. Using this series of compounds it in fact appears that the lattice parameter of $(BiY)Sn_2O_7$ is not unusually large, but rather that there is a negative deviation from Vegard's law for the Bi-rich compounds with $\delta > 1$. The structure of $(BiY)Sn_2O_7$ shows no evidence for any sterochemical influence of the Bi $6s^2$ electrons.

The structure of $(BiYb)Sn_2O_7$ was also studied using powder neutron diffraction. Like the Y analogue this compounds adopts the simple pyrochlore structure at room temperature although there is a considerable broadening of the Bragg reflections (Fig. 6) indicative of strain or particle size effects. This is despite the fact that the sample was annealed under identical conditions to those of $(BiY)Sn_2O_7$. The line broadening is believed to result mainly from strain induced by the size mismatch of the Yb-Bi ions. This strain does not induce a phase transition as the sample is cooled; $(BiYb)Sn_2O_7$ adopts the cubic pyrochlore structure between 10 and 295 K. The (BiYb)–O and (BiYb)–O′ distances systematically increase with increasing cell size. These compounds extend the data obtained for $(BiY)Sn_2O_7$ and further demonstrate the absence of a structural anomaly that can be ascribed to the $6s^2$ electrons. The Sn–O distance shows the greatest variation from a simple linear dependence with the cell size as a consequence of differences in the covalent Sn–O bonding (Table 6). Evidence for covalency in these compounds has been found in a study of the charge distribution of $Y_2Sn_2O_7$ using a Maximum Entropy Method (35).

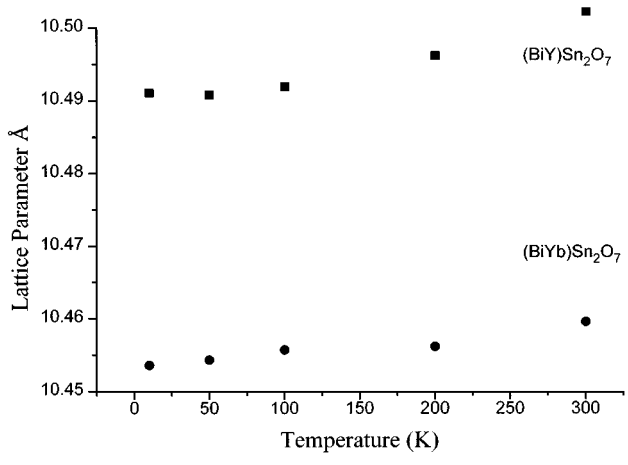

FIG. 5. Temperature dependent variation of the cubic lattice parameter for $(BiY)Sn_2O_7$ and $(BiYb)Sn_2O_7$.

For $(BiYb)Sn_2O_7$, as expected, the cell volume increases as the sample is heated. But now x is essentially independent of the cell size. This is in contrast to the behavior found for $(BiY)Sn_2O_7$ and in the general series $Ln_2M_2O_7$, $M =$ Sn, Ru. The temperature-dependent variation of the oxygen positional parameter in these complexes is very small, as seen for $(BiY)Sn_2O_7$ where x varies by less than 0.0005 over a 300° temperature range. We do not believe that the low value of x observed in $Bi_2Sn_2O_7$ is an artifact of the use of high-temperature in obtaining the cubic pyrochlore, but rather it reflects anomalous bonding interactions in this compound.

The temperature dependence of the Bi thermal displacement parameters are unremarkable; a small regular decrease with both temperature and cell volume is observed. We conclude that the Bi $6s^2$ electrons are spherically delocalized in both $(BiY)Sn_2O_7$ and $(BiYb)Sn_2O_7$ and that they have no unusual sterochemical influence.

TABLE 6
Selected Structural Properties of some Bi–Sn Pyrochlores

Compound	a (Å)	x	Sn–O (Å)	A–O (Å)	A–O′ (Å)	Reference
$Bi_2Sn_2O_7$	10.7438	0.3255	2.065	2.669	2.326	This work
$(BiY)Sn_2O_7$	10.5022	0.3323	2.045	2.560	2.273	This work
$Y_2Sn_2O_7$	10.3723	0.3369	2.043	2.495	2.246	21
$(BiYb)Sn_2O_7$	10.4661	0.3336	2.047	2.541	2.266	This work
$Yb_2Sn_2O_7$	10.3046	0.3391	2.040	2.463	2.231	20
R^a	–	0.9948	0.9686	0.9993	1.0000	

Note. Data refers to room temperature structure except for $Bi_2Sn_2O_7$ (850°C).
[a] Linear regression R values for dependence of property on the lattice parameter.

The electronic spectra of the various $(Bi_{2-\delta}Y_\delta)Sn_2O_7$ compounds show a number of differences. The UV spectrum of $Y_2Sn_2O_7$ shows a strong feature near 800 nm, a number of weaker features, and a high energy feature near 250 nm. The absorption band near 800 nm is the result of a Sn–O charge transfer (CT) process, the energy of which remains essentially unchanged as the Bi content is increased (Fig. 7). This is in agreement with the findings of Pannetier (36) and others (10, 37) that the B_2O_6 sublattice only weakly interacts with the A_2O' sublattice and demonstrates that in these compounds the small changes in the Sn–O distances have little effect on the comparative stability of the Sn(IV) cations. Three other important features seen in the electronic spectra are, first, that as the Bi content increases, the energy of the high-energy transition progressively decreases. We assign the feature near 250 nm to a Bi–O CT process and argue that this change is due to the easier formal reduction of Bi(III) as the Bi content increases. This can be understood in terms of a lengthening of the average Bi–O bond distance reducing the electron density on the Bi(III) cations. Second, it is obvious that the high-energy CT spectra of tetragonal $Bi_2Sn_2O_7$ is distinctly different from that of the cubic pyrochlores, and in particular the Bi–O CT band has moved to higher energies compared to $(Bi_{1.8}Y_{0.2})Sn_2O_7$. It may be postulated that in the tetragonal phase the Bi–O bond distances are somewhat shorter than those observed in the cubic pyrochlores, which has the effect of increasing the electron density on the Bi(III) making it energetically more difficult to formally reduce these. Finally, we observe that the shape of the Bi–O CT feature for $\delta = 0.2$ and 0.4, i.e., the two oxides where the Bi atoms is significantly displaced along the [111] direction, is noticeably different and displays both larger shifts and a splitting of the peaks.

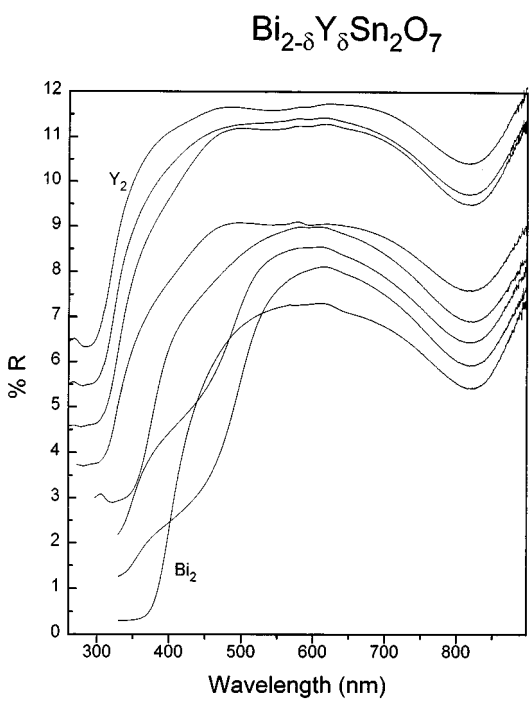

FIG. 7. Solid state electronic spectra for $(Bi_{2-\delta}Y_\delta)Sn_2O_7$ at room temperature.

We (18, 20, 38), and others (39–42), have demonstrated that bond valence sum (BVS) calculations are a convenient method to gain some insight into bonding changes over a series of closely related compounds. In the present work we have used BVS calculations to establish if there is a correlation between the observed structural variations and changes in the bonding as seen in the electronic spectra. Unfortunately, BVS calculations cannot consider variable site occupancies and so it was necessary to use ideal stoichiometric compounds with variable structural parameters. Site average BVS can, of course, be calculated; however these do not proportion charge differences between the two ions occupying the same site. A series of BVS calculations were performed assuming pure Bi or Y occupancy on the A site. Since the available data suggest an approximately linear relationship between a and x for Bi–Sn pyrochlores ($x = 0.65911 - 0.03109a$), this was used to estimate idealized structures. The results of some of these calculations are shown in Fig. 8.

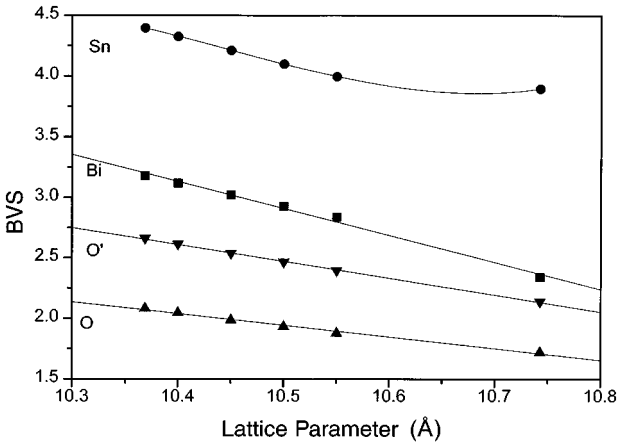

FIG. 8. Example of BVS calculation showing the evolution of bonding in $Bi_2Sn_2O_7$.

In the Bi compounds the short Bi–O′ distance increases as the lattice parameter increases, reducing the ability of the electropositive Bi(III) ion to gain electron density from the oxygens. The change in the oxygen positional parameter that accompanies the expansion in a is too small to prevent an increase in the six longer Bi–O bond distances. Thus, as the lattice expands, the Bi tends to become "underbonded" and the BVS drops appreciably below the ideal value of 3, being 2.337 in $Bi_2Sn_2O_7$.[1] The Madelung site potential is unusually high, -28.699 V, compared to values of around -31 V found in other Bi(III) oxides. Thus the stability of Bi(III) is lowered and reduction facilitated. This is confirmed by the decreased energy of the Bi–O CT band in the electronic spectra of the Bi-rich compounds. Conversely, if a Bi(III) ion is forced into a smaller lattice it can be "overbonded" with an effective BVS of well above 3. Oxidation of Bi(III) may be enhanced under these conditions; however no evidence for this is found in the electronic spectra and oxidation remains energetically unfavorable with respect to Bi(III) reduction. Indeed, although Bi(V) pyrochlores are known, it is generally found that the smaller Bi(V) cations occupy the pyrochlore B site rather than the A site (43–45). The changes in both the BVS and site potential are primarily a result of changes in the Bi–O′ bonding, although the BVS suggests (Fig. 8) that there is also a significant decrease in electron density on the O sites in the smaller lattice, indicative of stronger bonding. The BVS calculations suggest there is little change in the bonding of the Sn cations, again in accord with the electronic spectra. The same general trends are observed for the Y-containing pyrochlores—i.e., as the cell volume increases, the Y becomes underbonded, although this effect is much greater than for the Bi case. There are no low-energy CT bands in the electronic spectra corresponding to Y(III) reduction reflecting the greater stability of Y(III) compared to Y(0).

The above shows there is both a size and bonding limitation on the substitution of Bi into the $Y_2Sn_2O_7$ lattice. Conversely, in $Bi_2Sn_2O_7$ the Bi is already underbonded and the substitution of the smaller, weaker bonding Y ions is favored since this strengthens the Bi–O bond as a result of the lattice contraction. This may be the origin of the appreciable negative deviation from Vegard's law observed for the Bi-rich compounds. We suggest that the instability of the cubic pyrochlore structure in $Bi_2Sn_2O_7$ at room temperature is a consequence of an underbonding of the Bi(III) atoms and that the observed structural distortion acts to decrease the average Bi–O bond distance. Attempts are in progress to determine the precise structural properties of $Bi_2Sn_2O_7$ at room temperature to confirm this hypothesis.

What, if any, conclusions can be drawn with respect to catalysis? If we consider the pyrochlore lattice, then it is probable that the O′ atoms at the surface will be somewhat hydroxyl-like due to bonding with adsorbed water further increasing the electro-positive nature of the Bi(III) ions. Hence the surface Bi(III) atoms will provide an active site to bond any electronegative group. Furthermore, the larger cell volume of $Bi_2Sn_2O_7$ enables weak Lewis acids to occupy the tunnels in the pyrochlore lattice, further enhancing the catalytic behavior. This is in agreement with the observation that $Y_2Sn_2O_7$ is a less active catalyst than $Bi_2Sn_2O_7$ (4, 5). The fact that catalytic activity does not evolve in a continuous manner across the series $Ln_2Sn_2O_7$ suggests that additional interactions possibly involving the redox potential of the individual lanthanides on the B site are also important.

[1] This value is probably an underestimation since the structure was determined at 850°C and the value of R_0 used is appropriate for a room temperature structure.

ACKNOWLEDGMENTS

This work has utilized facilities through the support of the Australian Institute of Nuclear Science and Engineering, the Australian National Beamline Facility, and at BNL the U.S. Department of Energy. The support of the Australian Research Council is also acknowledged.

REFERENCES

1. T. Mallat, Z. Bodnar, P. Hug, and A. Bailker, *J. Catal.* **153,** 131 (1995).
2. M. Besson, F. Lahmer, P. Gallezot, P. Fuertes, and G. Fleche, *J. Catal.* **152,** 116 (1995).
3. T. R. Felthouse, P. B. Fraundorf, R. M. Friedman, and C. L. Schosser, *J. Catal.* **127,** 393 (1991).
4. D. J. Hucknall, "Selective Oxidation of Hydrocarbons." Academic Press, New York, 1974.
5. G. S. V. Coles, S. E. Bond, and G. Williams, *J. Mater. Chem.* **4,** 23 (1994).
6. G. Gokagac and B. J. Kennedy, *J. Electronanal. Chem.* **368**, 235 (1994).
7. J. B. Goodenougth, R. Manoharan, and M. Paranthaman, *J. Am. Chem. Soc.* **112,** 2076 (1990).

8. P. A. Cox, J. B. Goodenougth, P. J. Tavener, D. Telles, and R. G. Edgell, *J. Solid State Chem.* **62,** 360 (1986).
9. W. Y. Hsu, R. V. Kasowski, T. Miller, and T. C. Chiang, *Appl. Phys. Lett.* **52,** 7 (1988).
10. M. A. Subramanian, G. Aravamudan, and G. V. Subba Rao, *Progr. Solid State Chem.* **15,** 55 (1983).
11. C. A. Mims, A. J. Jacobson, R. B. Hall, and J. T. Lewandowski, *J. Catal.* **153,** 197 (1995).
12. J. T. Lewandowski, A. J. Jacobson, and R. B. Hall, "Synthesis and Properties of New Catalysts," p. 97. *Mat. Res. Soc.*, Boston, 1990.
13. G. S. V. Coles, K. J. Gallagher, and J. Wilson, *Sens. Actuators* **4,** 283 (1985).
14. C. A. Mims, A. J. Jacobson, R.B. Hall, and J. T. Lewandowski, *J. Catal.* **153,** 197 (1995).
15. R. D. Shannon, J. D. Bierlein, J. L. Gilson, G. A. Jones, and A.W. Sleight, *J. Phys. Chem. Solids* **41,** 117 (1980).
16. R. S. Roth, *J. Res. Natl. Bur. Std.* **56,** 17 (1956).
17. G. Vetter, F. Queyroux, and J. C. Gilles, *Mater. Res. Bull.* **13,** 211 (1978).
18. B. J. Kennedy and T. Vogt, *J. Solid State Chem.* **126,** 261 (1996).
19. G. R. Facer, M. M. Elcombe, and B. J. Kennedy, *Aust. J. Chem.* **46,** 1897 (1993).
20. B. J. Kennedy, B. A. Hunter, and C. J. Howard, *J. Solid State Chem.* **129** in press (1997).
21. G. R. Facer, C. J. Howard, and B. J. Kennedy, *Powder Diff.* **8,** 245 (1993).
22. B. J. Kennedy, *J. Solid State Chem.* **123,** 14 (1996).
23. R. F. Garrett, D. J. Cookson, G. J. Foran, T. M. Sabine, B. J. Kennedy, and S. W. Wilkins, *Rev. Sci. Instrum.* **66,** 1351 (1995).
24. T. M. Sabine, B. J. Kennedy, R. F. Garrett, G.J. Foran, and D.J. Cookson, *J. Appl. Cryst.* **28,** 513 (1995).
25. J. D. Axe, S. Cheung, D. E. Cox, L. Passell, and T. Vogt, *J. Neutron Res.* **2,** 85 (1994).
26. C. J. Howard, C. J. Ball, R. L. Davis, and M. M. Elcombe, *Aust. J. Phys.* **36,** 507 (1983).
27. J. Cockcroft, "PROFIL." Institut Laue Langevin, Grenoble, France, 1991.
28. R. J. Hill and C. J. Howard, Australian Atomic Energy Commission Report No. M 112, AAEC (now ANSTO), Lucas Heights Research Laboratories, New South Wales, Australia, 1986.
29. T. M. Sabine, unpublished work.
30. M. O'Keeffe, "EUTAX, Version 1.3." Emlab Software, Phonix, AZ, 1993.
31. G. Kreuzberg, F. Stewner, and R. Hoppe, *Z. Anorg. Allg. Chem.* **379,** 242 (1970).
32. F. Brisse and O. Knop, *Can. J. Chem.* **46,** 859 (1968).
33. A. K. Cheetham and N. Norman, *Acta Chem. Scand. A* **28,** 55 (1974).
34. E. Beck and S. Kemmler-Sack, *J. Less Common Metals* **135,** 257 (1987).
35. M. Sakata, M. Takata, C. J. Howard, and B. J. Kennedy, unpublished observations.
36. J. Pannetier, *J. Phys. Chem. Solids* **34,** 583 (1973).
37. R. A. McCauley, *J. Appl. Phys.* **51,** 290 (1980).
38. D. J. Buttrey, T. Vogt, U. Wildgruber, and W. R. Robinson, *J. Solid State Chem.* **111,** 118 (1994).
39. I. D. Brown and D. Altermatt, *Acta Crystallogr. B* **41,** 244 (1985).
40. I. D. Brown, *Acta Crystallogr. B* **48,** 553 (1992).
41. N. E. Brese and M. O'Keeffe, *Acta Crystallogr. B* **47,** 192 (1991).
42. J. L. Fourquet, H. Duroy, and P. Lacorre, *J. Solid State Chem.* **114,** 575 (1995).
43. N. Kumada, M. Hosoda, and N. Kinomura, *J. Solid State Chem.* **106,** 476 (1993).
44. J. Trehoux, F. Abraham, and D. Thomas, *Mater. Res. Bull.* **17,** 309 (1982).
45. J. Trehoux, F. Abraham, D. Thomas, C. Doremieux-Morin, and H. Arribart, *J. Solid State Chem.* **73,** 80 (1988).